Vehicle centre of mass, roll-centre and pitch-centre height estimation

Theunis R. Botha* and P. Schalk Els

Department of Mechanical and Aeronautical Engineering,
University of Pretoria,
Private Bag x20 Hatfield, 0028, South Africa
Email: theunis.botha@up.ac.za
Email: schalk.els@up.ac.za
*Corresponding author

Abstract: The location of a vehicle's centre of mass is an important parameter as it has a determining effect on the dynamics of a vehicle. The height of the vehicle centre of mass from the roll and pitch centres has a large influence on the load transfer which occurs between wheels during braking and cornering manoeuvres. These vehicle parameters can vary significantly especially on off-road vehicles due to the large differences in laden and unladen weight. This paper proposes an algorithm where suspension forces and inertial parameters are estimated in real time using inexpensive sensor measurements and an unscented Kalman filter. The algorithm is experimentally validated on an off-road vehicle performing various manoeuvres and driving over different terrains. The real time estimation of these parameters could contribute significantly to improving vehicle safety and control.

Keywords: centre of gravity estimation; suspension force estimation; roll centre height; pitch centre height.

Reference to this paper should be made as follows: Botha, T.R. and Els, P.S. (2019) 'Vehicle centre of mass, roll-centre and pitch-centre height estimation', *Int. J. Vehicle Systems Modelling and Testing*, Vol. 13, No. 4, pp.319–339.

Biographical notes: Theunis R. Botha received his PhD in Mechanical Engineering from the University of Pretoria, South Africa in 2015. His PhD work focused on using digital image correlations to perform vehicle measurement such as tyre slip angle and slip ratio using digital cameras. Currently, he is employed as a Senior Lecturer at the University of Pretoria, South Africa. His research interests are dynamics, integrated vehicle safety systems, autonomous vehicle control, mechatronics, parameter estimation and digital image correlation

P. Schalk Els worked in industry, developing and testing military wheeled vehicles for five years, where he was actively involved in new technology projects and applied research. Highlights include semi-active dampers for heavy vehicles, including the world's first semi-active hydraulic rotary damper (with Horstman Defence). In 1999, he joined the Department of Mechanical and Aeronautical Engineering at the University of Pretoria as a permanent staff member and obtained a PhD in 2006. His current research interests include semi-active dampers, semi-active springs and height adjustment to improve ride comfort, handling, rollover propensity and life of heavy off-road vehicles.

1 Introduction

Accurate real-time information on vehicle inertia properties, specifically the vehicle mass, centre of mass (CoM) location and the distance of the centre of mass to the roll and pitch centres, can greatly improve control algorithms related to braking, handling and vehicle safety. The vehicle mass and its lateral and longitudinal location have a significant effect on vehicle handling as it directly affects the handling characteristics of the vehicle (Gillespie, 1992; Jazar, 2017). While most stability controllers assume prior knowledge of the location of the centre of mass (Di Cairano et al., 2013; Rubin and Arogeti, 2015; Tchamna and Youn, 2013) the centre of mass position is not always constant and changes based on loading conditions. The loading conditions on passenger vehicles may not vary greatly between unladen and fully laden. However, on SUV, off-road as well as mining and agricultural vehicles the change is mass can be substantial and will have a significant effect on the handling of the vehicle.

The height of the centre of mass above the roll and pitch centre largely determines the load transfer which occurs as a result of the acceleration experienced by the vehicle body. Therefore, prior knowledge of the height of the mass above the roll and pitch centre, especially on SUV and off-road vehicles, can provide information on roll-over propensity of a vehicle. Therefore, real time estimation of these parameters can be incorporated into vehicle stability controllers and other safety systems to not only improve handling but safety as well.

The vehicle mass can be estimated using longitudinal dynamics of the vehicle but requires knowledge of the longitudinal forces or torques produced at the wheel (Yoon et al., 2007; Chu et al., 2013; Holm, 2011). The longitudinal force can be measured using wheel force transducers (WFT) but this is not a viable solution for commercial applications. The wheel torques can also be measured by measuring shaft torques. This solution while being more simplistic and cheaper than WFTs still requires the measurement of the torque on a rotating system. Recently the development of load sensing bearings (Madhusudhanan et al., 2016) also provide the ability to measure the forces at the tyre in a more compact and cost effective manner. While more cost effective the bearing unit is not standard and needs to be designed for. Long-term robustness of the system also needs to evaluate and the system may still not be cost effective for most vehicles at the moment. More elegant solutions make use of engine models which take into consideration multiple measurements such as the amount of fuel being injected into the cylinders to determine the engine torque. Using the vehicles gear ratios the wheel torques can be determined from the engine model. While the use of an engine model is very elegant, since as all measurements needed for it can be determined using the ECU in modern vehicles, it requires thorough knowledge of the engine to be able to develop such a model. The development of such an engine model is therefore difficult for anyone other than the OEM manufacturer of the engine to produce. Without knowledge of the longitudinal force the use of the longitudinal vehicle dynamics to determine the vehicle mass is impossible. Also while these systems can estimate the vehicle mass these methodologies are incapable of determining the location of the centre of mass and therefore the effect the change of mass has on the handling of the vehicle.

An alternative method by Kim et al. (2013) uses the lateral motion of the vehicle to estimate the vehicle mass. In the formulation the steer angle of the vehicle is used to determine, by means of linear lateral tyre model, the lateral force produced by the tyres. Using the estimated lateral force the vehicles mass can be estimated. The main drawback of this approach is that the linear tyre model is used which neglects changes in the tyre condition, effects of load transfer and saturation of the tyre force. The method also assumes that there are no vertical excitations of the tyre. Therefore, the system will not work when diving over terrain which induces vertical excitations of the vehicle. Huang and Wang (2012) also make use of a known tyre model to perform vehicle inertial property estimation and motion control. The authors note that the cornering stiffness of the tyre can be estimated using other techniques (Hahn et al., 2002). The study is however only validated using simulation data. Rozyn and Zhang (2010) developed a method based on the free decay responses of the vehicle over discrete objects of unknown dimensions. The method makes use of a simplified vertical vibration model of the vehicle and modal analysis techniques are used to determine the sprung mass frequency, damping ratio and mode shapes. The technique shows promise but has not been tested on experimental data to evaluate the robustness of the estimator.

The height of the sprung mass above the roll centre is often estimated based on the roll angle of the vehicle body (Solmaz et al., 2008). In this approach the roll angle is estimated using sensor measurements and a basic vehicle model which makes assumptions on the mass and the cornering stiffness of the tyre. The theory is that the roll angle of the body is dependent on the experienced lateral acceleration and the height of the unsprung centre of mass above the roll centre. The assumptions of a the linear tyre model, damper and spring limits the accuracy of the method and the assumption of a known unsprung mass limits its viability of a real-time estimation in changing loading conditions.

Sandu et al. (2015) proposed an estimation technique where the weight distribution and centre of mass height above roll and pitch centres are estimated using a load transfer model. However, in Sandu et al. (2015), the strut forces are measured using a pressure sensor as the vehicle is equipped with a hydro-pneumatic suspension system. While this provides a direct measurement of the strut forces, neglecting friction, this method is not possible in most vehicles. Huang and Wang (2013) proposed a similar method whereby the centre of mass height is estimated using a load transfer model. In this study the vertical force on the tyres are estimated using the effective roll radius of the tyre. The roll radius is estimated using the instantaneous angular velocity of the tyre and the wheel centre velocity. The change in roll radius can be used to estimate the vertical load change using the vertical tyre stiffness. The measurement of the wheel centre velocity is based on GPS measurements which are known to have delays of up to 150 ms. The GPS delay and the accuracy of measuring the change is roll radius affect the robustness of this method. The vertical stiffness is also dependent on the tyre pressure and the method assumes a known mass of the vehicle.

The current paper builds on the work by Sandu et al. (2015). Instead of directly measuring the suspension forces the suspension displacement and velocity is estimated using a kinematics-based estimator and suspension model. The estimated values are

supplied as inputs to a suspension model to determine the strut forces. The weight distribution and roll and pitch centre height is subsequently estimated using an unscented Kalman filter. The estimation technique is experimentally validated using experimental data.

2 Strut force estimation

The force in each corner of the vehicle is estimated using a mathematical model of the suspension system which takes as input the vertical displacements and velocities of the sprung and unsprung mass at each corner of the vehicle. The model can include aspects such as kinematics and compliance or just the spring and damper forces. The more representative the model is of the actual suspension system, the more accurate the estimation of the strut forces will be. However, these models are generally easy to develop as they are required for any vehicle simulation. The estimation of the strut force revolves around the estimation of the relative displacement and velocity between the sprung and unsprung mass at each corner. The measurements used for the estimation is the relative displacement between the sprung and unsprung mass at each corner, the vertical acceleration of the unsprung and sprung mass, as well as, the roll and pitch velocities of the sprung mass. These measurements can easily be obtained from inexpensive sensors and several of them are already included on most modern vehicles. The estimation is performed using a linear Kalman filter. The Kalman filter (Kalman, 1960) was introduced as a filtering method to reduce noise in a linear system which can be described by means of a state transition equation. The filter consists of a time update or prediction step and a measurement update or correction step. The filter represents an optimal filter under the assumptions of a linear system with white noise i.e. additive Gaussian noise with zero mean and variance Q. The assumption of white noise, while not always true, is an acceptable assumption in most circumstances.

Figure 1 Description of states used in kinematic estimators

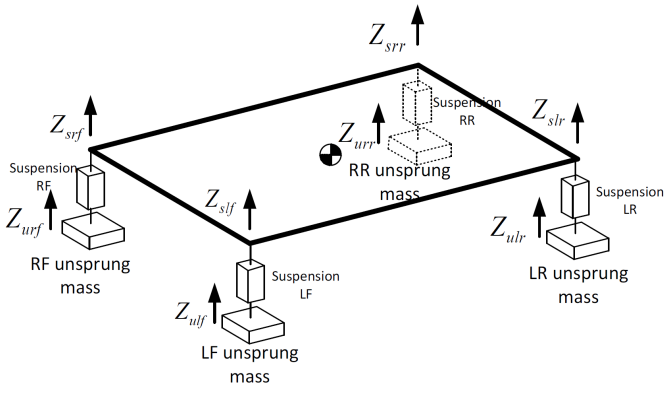

A kinematic estimation model is used in the Kalman filter to estimate the displacement and velocity of the sprung and unsprung mass at each corner of the vehicle. The state vector is given as:

$$\boldsymbol{X} = \left[Z_{ulf}\ \dot{Z}_{ulf}\ Z_{urf}\ \dot{Z}_{urf}\ Z_{ulr}\ \dot{Z}_{ulr}\ Z_{urr}\ \dot{Z}_{urr}\ Z_{slf}\ \dot{Z}_{slf}\ Z_{srf}\ \dot{Z}_{srf}\ Z_{slr}\ \dot{Z}_{slr}\ Z_{srr}\ \dot{Z}_{srr} \right]^T \quad (1)$$

Z_{aij} with $a = u, s$ representing the unsprung or sprung mass respectively $i = l, r$ representing the left or right side of the vehicle respectively and $j = f, r$ representing the front or rear of the vehicle respectively. Figure 1 shows the description of the states used in the kinematic estimator.

The state transition model for each displacement and velocity combination is given as

$$\boldsymbol{X}_k = \boldsymbol{F}\boldsymbol{X}_{k-1} + \boldsymbol{B}\boldsymbol{U}_k \quad (2)$$

$$\begin{bmatrix} Z_{aij} \\ \dot{Z}_{aij} \end{bmatrix}_k = \begin{bmatrix} 1 & \Delta t \\ 0 & 1 \end{bmatrix} \begin{bmatrix} Z_{aij} \\ \dot{Z}_{aij} \end{bmatrix}_{k-1} + \begin{bmatrix} \frac{1}{2}\Delta t^2 \\ \Delta t \end{bmatrix} \ddot{Z}_{aij} \quad (3)$$

where $\ddot{Z}_{aij}$ is the measured vertical acceleration at corner ij either on the sprung mass ($a = s$) or the unsprung mass ($a = u$). The vertical acceleration measurements and equations of the unsprung mass can be removed if the vehicle is driven over smooth terrain where the motion of the unsprung mass can be neglected. However for completeness the motion of the unsprung mass is included. The correction phase of the Kalman filter uses the relative displacements and velocities between the sprung and unsprung mass given as:

$$\delta_{ij} = Z_{sij} - Z_{uij} \quad (4)$$

$$\dot{\delta}_{ij} = \dot{Z}_{ij} - \dot{Z}_{uij} \quad (5)$$

The relative velocity is estimated using finite differences. It should be noted that this measurement is very noisy and therefore is given a high uncertainty in the filter but the addition of this measurement helps to reduce the drift in the velocity estimates.

Additionally the roll and pitch velocities are used as correction measurements. It can be shown that the roll $(\dot{\theta}_r)$ and pitch $(\dot{\theta}_p)$ velocity of the vehicle can be determined from the velocities of the corners as:

$$\dot{\theta}_r = \frac{\dot{Z}_{slf} - \dot{Z}_{srf}}{l_w} \quad (6)$$

$$\dot{\theta}_r = \frac{\dot{Z}_{slr} - \dot{Z}_{srr}}{l_w} \quad (7)$$

$$\dot{\theta}_p = \frac{\dot{Z}_{slr} - \dot{Z}_{slf}}{l} \quad (8)$$

$$\dot{\theta} = \frac{\dot{Z}_{srr} - \dot{Z}_{srf}}{l} \quad (9)$$

As none of these parameters corrects the global position of any of the points, an additional measurement, in the form of an artificial unsprung mass vertical position of 0, is provided at each corner. These measurements are given a high covariance or high

uncertainty and are only used to slowly remove the drift of the displacements. The full measurement update equation is:

$$\boldsymbol{Y}_k = \boldsymbol{H}\boldsymbol{X}_k \tag{10}$$

$$\boldsymbol{Y}_k = \begin{bmatrix} \delta_{lf} \\ \delta_{rf} \\ \delta_{lr} \\ \delta_{rr} \\ \dot{\theta}_r \\ \dot{\theta}_r \\ \dot{\theta}_p \\ \dot{\theta}_p \\ \dot{\delta}_{lf} \\ \dot{\delta}_{rf} \\ \dot{\delta}_{lr} \\ \dot{\delta}_{rr} \\ 0 \\ 0 \\ 0 \\ 0 \end{bmatrix} = \begin{bmatrix} -1 & 0 & 0 & 0 & 0 & 0 & 0 & 0 & 1 & 0 & 0 & 0 & 0 & 0 & 0 & 0 \\ 0 & 0 & -1 & 0 & 0 & 0 & 0 & 0 & 0 & 0 & 1 & 0 & 0 & 0 & 0 & 0 \\ 0 & 0 & 0 & 0 & -1 & 0 & 0 & 0 & 0 & 0 & 0 & 0 & 1 & 0 & 0 & 0 \\ 0 & 0 & 0 & 0 & 0 & 0 & -1 & 0 & 0 & 0 & 0 & 0 & 0 & 0 & 1 & 0 \\ 0 & 0 & 0 & 0 & 0 & 0 & 0 & 0 & 0 & l_w & 0 & -l_w & 0 & 0 & 0 & 0 \\ 0 & 0 & 0 & 0 & 0 & 0 & 0 & 0 & 0 & 0 & 0 & 0 & 0 & l_w & 0 & -l_w \\ 0 & 0 & 0 & 0 & 0 & 0 & 0 & 0 & 0 & -l & 0 & 0 & 0 & l & 0 & 0 \\ 0 & 0 & 0 & 0 & 0 & 0 & 0 & 0 & 0 & 0 & 0 & -l & 0 & 0 & 0 & l \\ 0 & -1 & 0 & 0 & 0 & 0 & 0 & 0 & 0 & 1 & 0 & 0 & 0 & 0 & 0 & 0 \\ 0 & 0 & 0 & -1 & 0 & 0 & 0 & 0 & 0 & 0 & 0 & 1 & 0 & 0 & 0 & 0 \\ 0 & 0 & 0 & 0 & 0 & -1 & 0 & 0 & 0 & 0 & 0 & 0 & 0 & 1 & 0 & 0 \\ 0 & 0 & 0 & 0 & 0 & 0 & 0 & -1 & 0 & 0 & 0 & 0 & 0 & 0 & 0 & 1 \\ 1 & 0 & 0 & 0 & 0 & 0 & 0 & 0 & 0 & 0 & 0 & 0 & 0 & 0 & 0 & 0 \\ 0 & 0 & 1 & 0 & 0 & 0 & 0 & 0 & 0 & 0 & 0 & 0 & 0 & 0 & 0 & 0 \\ 0 & 0 & 0 & 0 & 1 & 0 & 0 & 0 & 0 & 0 & 0 & 0 & 0 & 0 & 0 & 0 \\ 0 & 0 & 0 & 0 & 0 & 0 & 1 & 0 & 0 & 0 & 0 & 0 & 0 & 0 & 0 & 0 \end{bmatrix} \begin{bmatrix} Z_{ulf} \\ \dot{Z}_{ulf} \\ Z_{urf} \\ \dot{Z}_{urf} \\ Z_{ulr} \\ \dot{Z}_{ulr} \\ Z_{slf} \\ \dot{Z}_{slf} \\ Z_{srf} \\ \dot{Z}_{srf} \\ Z_{slr} \\ \dot{Z}_{slr} \\ Z_{srr} \\ \dot{Z}_{srr} \end{bmatrix} \tag{11}$$

From the state vector, the relative displacements and velocities can be determined from equations (4) and (5). The relative displacements and velocities can be used to determine the suspension forces using a suitable suspension model

$$F_{zij} = f\left(\delta_{ij}, \dot{\delta}_{ij}\right) \tag{12}$$

Since all of the equations presented are linear, the linear Kalman filter is the optimal filter to use under the assumption of Gaussian distributions.

3 Vehicle parameter estimation

During dynamic manoeuvres the forces experienced at the tyres or suspension changes. The change in force is a result of the forces which are generated between the tyres and the road if aerodynamic forces are ignored. The vehicle accelerates under the application of the external forces, resulting in a change of position of the centre of mass and a redistribution of the external forces between the wheels. The resulting change in vertical force on the wheels is often called load transfer.

Figure 2 depicts the roll degree of freedom of the vehicle, indicating the suspension forces as well as the roll centre. Figure 2(a) indicates the front view and Figure 2(b) shows an isometric view of the roll degree of freedom showing the roll axis of the vehicle. The vehicle is modelled using distributed point masses, with one mass at each corner of the vehicle. This method neglects the effect on the mass moment of inertia in

the roll and pitch directions. This reduces the estimation accuracy of the vehicle parameters during sudden motions where there may be high roll or pitch accelerations. However, these events are fairly short in duration and have a small effect on the load distribution. The use of point masses simplifies the load transfer model as will be seen later. Using the diagrams the roll degree of freedom is modelled by taking moments about the roll center. The reason for this is that the roll centre is viewed as the point at which the suspension link forces, generated by the forces at the tyre, act on the body. Therefore, taking moments about this point removes the suspension link forces from the analysis making the formulation simpler. The validity of these assumptions will be evaluated later when the experimental results are discussed.

Figure 2 Roll degree of freedom, (a) front view (b) isometric view

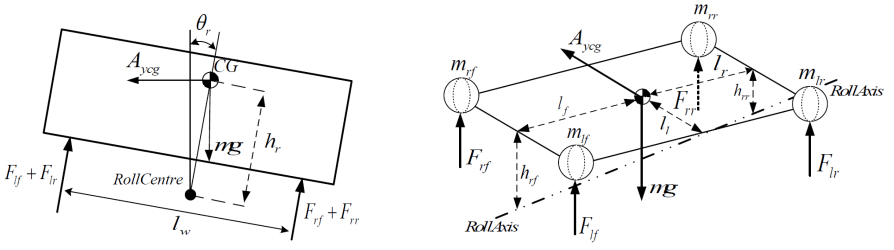

(a) (b)

The load transfer during lateral movement, which results from a lateral acceleration, in its simplest form is given as:

$$\Delta F_z = \frac{m\,\mathrm{A}_{\mathrm{yCoM}}\,h_r}{l_w} \tag{13}$$

where m the mass of the sprung mass is $\mathrm{A}_{\mathrm{yCoM}}$ is the lateral acceleration of the centre of mass, h_r is the height of the centre of mass of the body above the roll centre and l_w is the track width of the vehicle. This can similarly performed in the pitch direction for the vehicle. If the roll and pitch effects are incorporated the vertical suspension force at each corner can be determined as:

$$F_{zlf} = m_{lf}\ddot{Z}_{lf} - \frac{m_{lf}+m_{rf}}{l_w}A_{y\mathrm{CoM}}h_{rf} - \frac{m_{lf}+m_{lr}}{l_f+l_r}A_{x\mathrm{CoM}}h_{pf} \tag{14}$$

$$F_{zrf} = m_{rf}\ddot{Z}_{rf} - \frac{m_{lf}+m_{rf}}{l_w}A_{y\mathrm{CoM}}h_{rf} - \frac{m_{rf}+m_{rr}}{l_f+l_r}A_{x\mathrm{CoM}}h_{pf} \tag{15}$$

$$F_{zlr} = m_{lr}\ddot{Z}_{lr} - \frac{m_{lr}+m_{rr}}{l_w}A_{y\mathrm{CoM}}h_{rr} - \frac{m_{lf}+m_{lr}}{l_f+l_r}A_{x\mathrm{CoM}}h_{pl} \tag{16}$$

$$F_{zrr} = m_{rr}\ddot{Z}_{rr} - \frac{m_{lr}+m_{rr}}{l_w}A_{y\mathrm{CoM}}h_{rr} - \frac{m_{rf}+m_{rr}}{l_f+l_r}A_{x\mathrm{CoM}}h_{pr} \tag{17}$$

where F_{zij} is the vertical suspension force at location ij, m_{ij} is the point mass at each corner of the vehicle h_{rj} are the roll centres and h_{pi} are the pitch centres. The masses (m_{ij}) are used to determine the horizontal location of the centre of mass as:

$$l_f = \frac{\left(m_{lr} + m_{rr}\right)}{m_{lr} + m_{rr} + m_{lf} + m_{rf}} l \tag{18}$$

$$l_l = \frac{\left(m_{rf} + m_{rr}\right)}{m_{lr} + m_{rr} + m_{lf} + m_{rf}} l_w \tag{19}$$

The estimated centre of mass is only of the sprung mass However, in vehicle control systems the system requires information of the sprung mass only. Also, since the usprung mass locations and magnitudes almost never change the overall centre of mass location can be determined easily if the sprung mass in known.

Equations (14)–(17) require that the longitudinal and lateral accelerations be measured at the centre of mass of the vehicle sprung mass. This however is difficult to achieve if the location of the centre of mass is not known in advance. An estimate of these accelerations can be made by using 3-axis accelerometers at the 4 corners of the vehicle. The accelerometer readings can either be averaged or the current centre of mass position estimate can be used to determine the acceleration at the centre of mass. The roll and pitch centres are separated for the front and rear of the vehicle as the front and rear suspensions are generally not the same. The lateral load transfer in the front is only based on the mass at the front of the vehicle, i.e., m_{lf} + m_{rf} and vice versa. Similarly the longitudinal weight transfer on the left is based only on the mass on the left, i.e., m_{lf} + m_{lr} and the longitudinal weight transfer on the right is based only on the mass on the right. This formulation improves the load transfer model due to the differences in front and rear roll and left and right pitch centres and compensated for the compliance of the sprung mass (vehicle body).

The masses and roll/pitch centres is estimated using the unscented Kalman filter (UKF) (Julier and Uhlmann, 1995, 1997). The linear Kalman filter is the optimal filter with a linear system, however, since equations (14)–(17) are not linear, a nonlinear estimator should be used.

The extended Kalman filter (EKF) was introduced to handle nonlinear systems by linearising the system and by making use of a Jacobian matrix. The shortcomings of the EKF are that it approximates the state distribution by means of a linearised function, which can lead to incorrect estimation in severe nonlinear problems. The UKF was introduced to improve the state estimation in nonlinear systems by using a minimal set of carefully chosen sample points. These sample points are propagated through the true nonlinear system and can capture the posterior mean and covariance accurately to the second order (Taylor series expansion) for any nonlinearity.

The formulation of the UKF is as follows. Given a state vector $\boldsymbol{x}_k$, where k represents the time step, the initial conditions are:

$$\hat{\boldsymbol{x}}_0 = \mathrm{E}\left[\boldsymbol{x}_0\right] \tag{20}$$

$$\boldsymbol{P}_0 = \mathrm{E}\left[\left(\boldsymbol{x}_0 - \hat{\boldsymbol{x}}_0\right)\left(\boldsymbol{x}_0 - \hat{\boldsymbol{x}}_0\right)^T\right] \tag{21}$$

At the beginning of the prediction step, the sigma points $\boldsymbol{\chi}_{k-1}$ are determined by:

$$\boldsymbol{\chi}_{k-1} = \left[\hat{\boldsymbol{x}}_{k-1} \; \hat{\boldsymbol{x}}_{k-1} + \gamma\sqrt{\boldsymbol{P}_{k-1}} \; \hat{\boldsymbol{x}}_{k-1} - \gamma\sqrt{\boldsymbol{P}_{k-1}} \right] \tag{22}$$

where $\gamma = \sqrt{L+\lambda}$, L is the state vector length and λ is a composite scaling parameter calculated as $\lambda = \alpha^2(L+\kappa) - L$. α determines the spread of the sigma points and is usually set to a small positive value and κ is normally set to 0 or $L-3$.

The propagated sigma points, $\boldsymbol{\chi}^*_{k|k-1}$, are determined by:

$$\boldsymbol{\chi}^*_{k|k-1} = \mathbf{F}\left(\boldsymbol{\chi}_{k-1}, \mathbf{U}_{k-1}\right) \tag{23}$$

where **F** is the state transition function or process model and **U** are the inputs to the system. The a priori state estimation $\hat{\boldsymbol{x}}_k^-$ is approximated using a weighted sample mean:

$$\hat{\boldsymbol{x}}_k^- = \sum_{i=0}^{2L} W_i^m \chi^*_{i,k|k-1} \tag{24}$$

with weights W_i^m:

$$W_0^m = \lambda/(L+\lambda) \tag{25}$$

$$W_i^m = 1/(2(L+\lambda)) \tag{26}$$

The covariance matrix is:

$$\boldsymbol{P}_k^- = \sum_{i=0}^{2L} W_i^c \left[\chi^*_{i,k|k-1} - \hat{\boldsymbol{x}}_k^- \right]\left[\chi^*_{i,k|k-1} - \hat{\boldsymbol{x}}_k^- \right]^T + \boldsymbol{R}_v \tag{27}$$

The matrix $\boldsymbol{R}_v$ is the process noise covariance with weights W_i^c:

$$W_0^c = \frac{\lambda}{L+\lambda} + \left(1 - \alpha^2 + \beta\right) \tag{28}$$

$$W_i^c = 1/(2(L+\lambda)) \tag{29}$$

The value β is used to incorporate knowledge of the state distribution. For the case of Gaussian distribution, $\beta = 2$ is optimal.

The correction step starts with redrawing the sigma points using the state vector and covariance matrix from the predicted step:

$$\boldsymbol{\chi}_{k|k-1} = \left[\hat{\boldsymbol{x}}_k^- \quad \hat{\boldsymbol{x}}_k^- + \gamma\sqrt{\boldsymbol{P}_k^-} \quad \hat{x}_k^- - \gamma\sqrt{\boldsymbol{P}_k^-} \right] \tag{30}$$

The sigma points are propagated through the observation function and the mean calculated as:

$$\boldsymbol{\gamma}_{k|k-1} = \mathbf{H}\left(\boldsymbol{\chi}_{k|k-1}\right) \tag{31}$$

$$\hat{\boldsymbol{y}}_k^- = \sum_{i=0}^{2L} W_i^m \gamma_{i,k|k-1} \tag{32}$$

The measure and cross-covariance matrices are:

$$\boldsymbol{P}_{\hat{y}_k \hat{y}_k} = \sum_{i=0}^{2L} W_i^c \left[\gamma_{i,k|k-1} - \hat{\boldsymbol{y}}_k^- \right] \left[y_{i,k|k-1} - \hat{\boldsymbol{y}}_k^- \right]^T + \boldsymbol{R}_n \tag{33}$$

$$\boldsymbol{P}_{x_k y_k} = \sum_{i=0}^{2L} W_i^c \left[\chi_{i,k|k-1} - \hat{\boldsymbol{x}}_k^- \right] \left[\gamma_{i,k|k-1} - \hat{\boldsymbol{y}}_k^- \right]^T \tag{34}$$

The matrix $\boldsymbol{R}_n$ is the measurement noise covariance. The Kalman gain is computed as:

$$\boldsymbol{\varkappa}_k = \boldsymbol{P}_{x_k y_k} \boldsymbol{P}_{\hat{y}_k \hat{y}_k}^{-1} \tag{35}$$

The correction to the state is:

$$\hat{\boldsymbol{x}}_k = \hat{\boldsymbol{x}}_k^- + \boldsymbol{\varkappa}_k \left(\boldsymbol{y}_k - \hat{\boldsymbol{y}}_k^- \right) \tag{36}$$

where $\boldsymbol{y}_k$ is the vector containing actual observations or measurements from sensors. The covariance update equation is:

$$\boldsymbol{P}_k = \boldsymbol{P}_k^- - \boldsymbol{\varkappa}_k \boldsymbol{P}_{\hat{y}_k \hat{y}_k} \boldsymbol{\varkappa}_k \tag{37}$$

The state vector used in the UKF is:

$$\varkappa_k = \left[F_{zlf} \quad F_{zrf} \quad F_{zlr} \quad F_{zrr} \quad F_{zbounce} \quad m_{lf} \quad m_{lf} \quad m_{lf} \quad m_{lf} \quad h_{rf} \quad h_{rr} \quad h_{pl} \quad h_{pr} \right]^T \tag{38}$$

where $F_{zbounce} = F_{zlf} + F_{zrf} + F_{zlr} + F_{zrr}$.

The input vector used in the state propagation model is:

$$\mathbf{U}_k = \left[\ddot{Z}_{lf} \quad \ddot{Z}_{lf} \quad \ddot{Z}_{lf} \quad \ddot{Z}_{lf} \quad A_{x\mathrm{CoM}} \quad A_{y\mathrm{CoM}} \quad \ddot{Z}_{\mathrm{CoM}} \right]^T \tag{39}$$

The state propagation model $\mathbf{F}(\boldsymbol{\chi}_{k-1}, \mathbf{U}_{k-1})$ is defined as the four strut vertical forces from equations (14)–(17). With the additional equations for the other states defined as:

$$F_{zbounce,k} = F_{zlf,k} + F_{zrf,k} + F_{zlr,k} + F_{zrr,k} \tag{40}$$

$$m_{ij,k} = m_{ij,k-1} \tag{41}$$

$$h_{ri,k} = h_{ri,k-1} \tag{42}$$

$$h_{pj,k} = h_{pj,k-1} \tag{43}$$

The measurement correction step vector is:

$$y_k = \left[F_{zlf} \quad F_{zrf} \quad F_{zlr} \quad F_{zrr} \quad F_{zbounce} \right]^T \tag{44}$$

The measurements are the estimated vertical forces in the suspension obtained from equation (12).

4 Experimental results

The estimators are validated using experimental data measured on a Land Rover Defender. The vehicle is equipped with a hydro-pneumatic suspension system which

incorporates the damping and spring component into a single strut. The suspension model used in equation (12) is the sum of the spring and damper force. The spring characteristic is obtained by the compression of the gas and is modelled using an ideal gas formulation. A curve fit of experimental data is used to model the damping characteristic. The use of a hydro-pneumatic suspension system allows the strut force (combined spring and damping force) to be measured using a pressure transducer. It should be noted that the measurement does not include the friction in the system which can be as high as 500 N. The force, calculated from the pressure, is not used in the estimator, but only for comparison of the estimated suspension force. Various tests are used for validating the estimator under different driving conditions. These tests were conducted at different times with different instrumentation and different measurement setups between tests.

4.1 Belgian paving

The first test used for validation is the vehicle driving over rough Belgian paving at a constant speed of 20 km/h. The test is repeated multiple times from start to finish to see whether estimation results are constant. This test mainly excites the vertical motion of the unsprung mass and is a good validator of the suspension force estimator as the vehicle experienced random excitation from the road. The test was conducted at a vehicle proving ground with outriggers mounted on the front and rear of the vehicle for safety reasons. The mass which is added to the sprung mass by the outriggers was measured before testing and taken into account.

Figure 3 Measured vs. estimated suspension displacement and velocity over Belgian paving (see online version for colours)

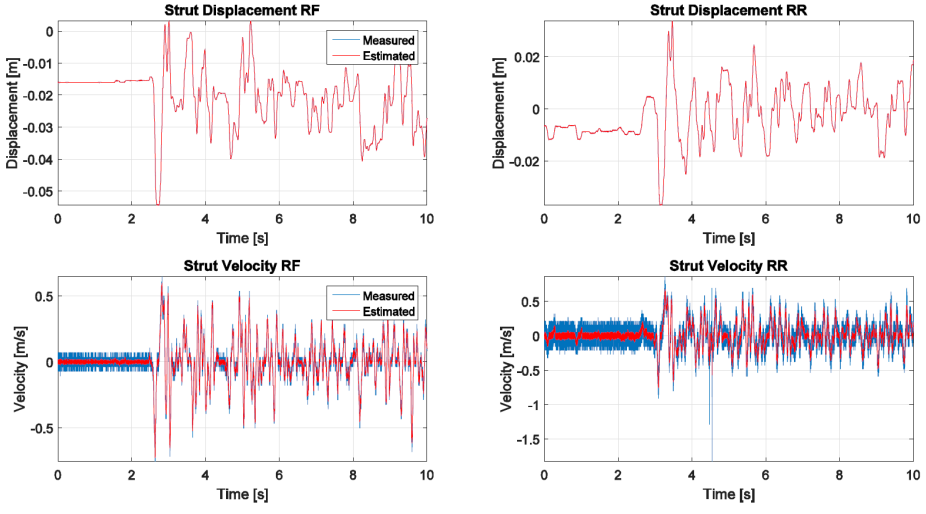

Figure 3 shows the displacement and velocity estimation of the right front and rear right strut. The inputs to the kinematic estimator are the accelerations of the unsprung and sprung mass at each corner, the measured suspension displacement, roll and pitch velocity. The outputs are the relative suspension displacement and velocity. The displacement estimate is exactly the same as the measured displacement. This is expected since the measurement has a low uncertainty. The velocity estimates are compared to

differentiated displacement measurements. Agreement is excellent but the estimate contains significantly less noise. While the same result can be obtained with a frequency-based filter, the filter will delay the obtained measurements. A frequency based filter will also have undesirable effect when there are short duration (high frequency) inputs.

Figure 4 Suspension force calculated from pressure measurements vs. estimated suspension force over Belgian paving (see online version for colours)

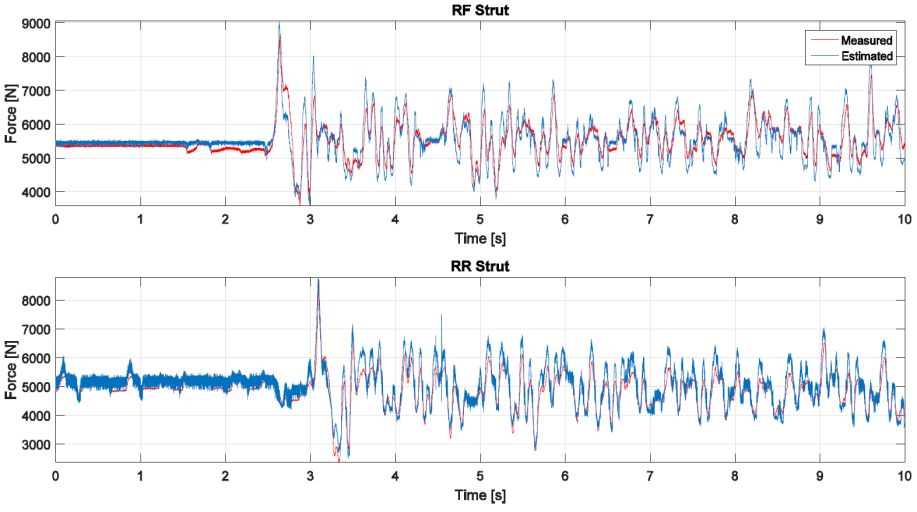

Figure 4 shows the estimation of the suspension force of the right front and right rear struts. Overall good correlation is achieved between measurements and estimates. Slight deviation can be due to suspension model inaccuracies since the exact gas volume in the suspension is not exactly known. The estimated force is slightly noisier than the measured force calculated from the pressure. This can partly be due to the measured force not including the friction component but also slight noise in the velocity measurement. Figure 5 shows the parameter estimation results. It can clearly be seen that the estimated and measured centre of mass and total mass estimates are very accurate. The maximum longitudinal position error during the duration of the test (neglecting the first few seconds of the estimation) is just over 3%, the lateral error is less than 3% and the error on the total sprung mass is less 6%. Therefore, it can be concluded that the estimator estimated the inertial parameters very accurately over a random rough terrain. During the test short periods of longitudinal acceleration are experienced before and after the Belgian paving. This allows the pitch roll centres' to estimated, there was no lateral acceleration measurement during the test and therefore no roll centres' estimated. The estimated take long to estimate due to the very short periods of longitudinal excitation. There is slight variation due to the noise in the acceleration due to crossing very rough terrain. The mean, standard deviation and maximum deviation of the estimated of the pitch centres', after convergence are shown in Table 1. From the results, the maximum deviation from the mean is only 15 mm. The exact pitch center heights ares difficult to compare to known values since there is very little theory about approximating the pitch center from suspension geometry in literature. As such no conclusion about the accuracy of these estimates can be made.

Figure 5 Actual vs. estimated parameters over the Belgian paving (see online version for colours)

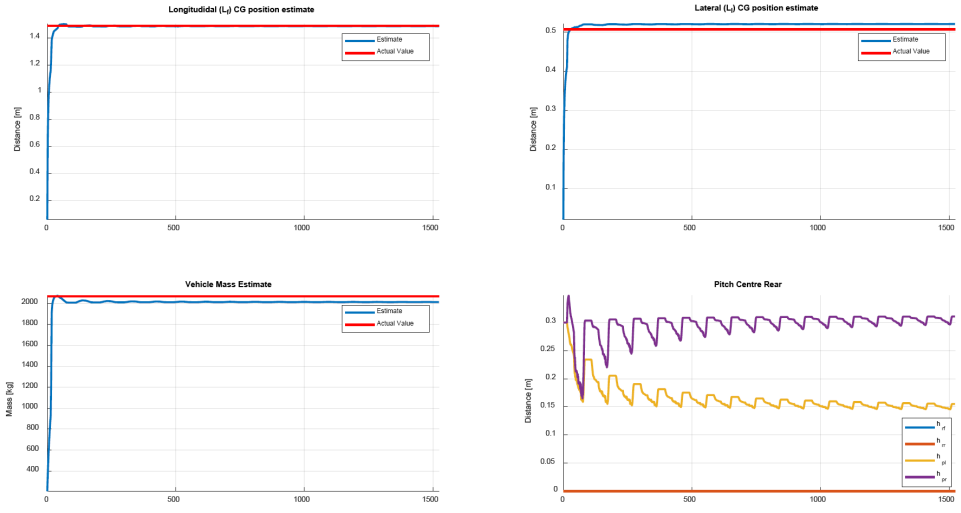

Table 1 Mean, standard deviation and maximum deviation of estimated for the left and right pitch centre heights while driving over Belgian paving

	h_{pl} *[m]*	h_{pr} *[m]*
Mean	0.152	0.305
Standard deviation	0.004	0.005
Maximum deviation	0.0073	0.015

4.2 Double lane change

A severe double lane change (DLC) accident avoidance manoeuvre, where the vehicle makes two sudden lane changes, was conducted according to ISO 3888-1 (International Organisation for Standardisation, 1999). The vehicle never obtains a steady state condition during this manoeuvre. The test is often used to evaluate roll over and handling of a vehicle. Figure 6 compares the measured and estimated displacement and velocity of the left and right rear struts for the vehicle performing a DLC with an entry speed of 80 km/h. The plots show good estimation of the displacement and velocity. For this test a load cell was connected between the left rear strut and the unsprung mass. This measurement thus measured the total strut force including friction. Figure 7 shows the suspension force. From the left rear strut it is evident that the load cell measurements are indeed noisier than the pressure sensor measurements. It can be concluded that some of the noise in the force estimation is indeed due to the friction component in the suspension system. It should be noted that the friction in this prototype system is higher than typical suspension friction in most passenger vehicle suspension system. However, part of the noise is still expected to be due to the slightly noisier velocity measurements. It is expected that this technique will work better on a vehicle with traditional suspension where the friction component can be neglected.

Figure 6 Measured vs. estimated strut displacement and velocity during a DLC at 80 km/h (see online version for colours)

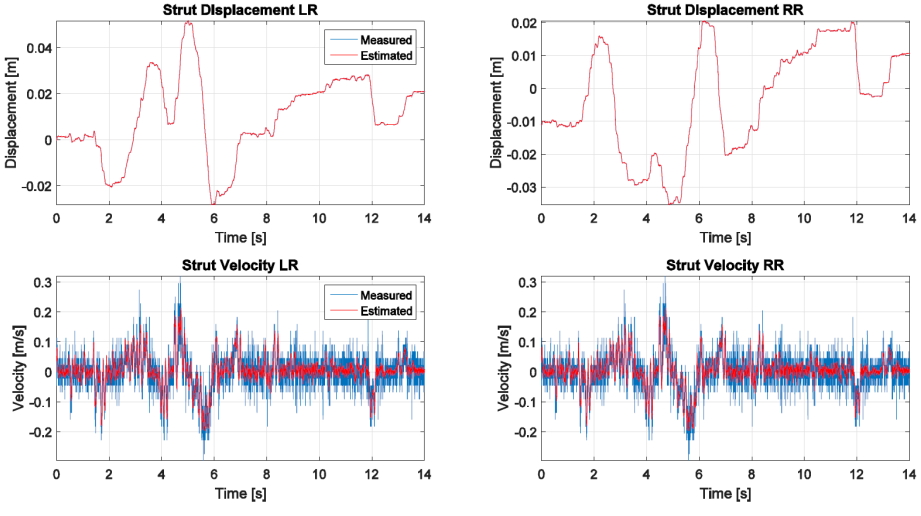

Figure 7 Experimental results of the estimated strut forces during a DLC at 80 km/h (see online version for colours)

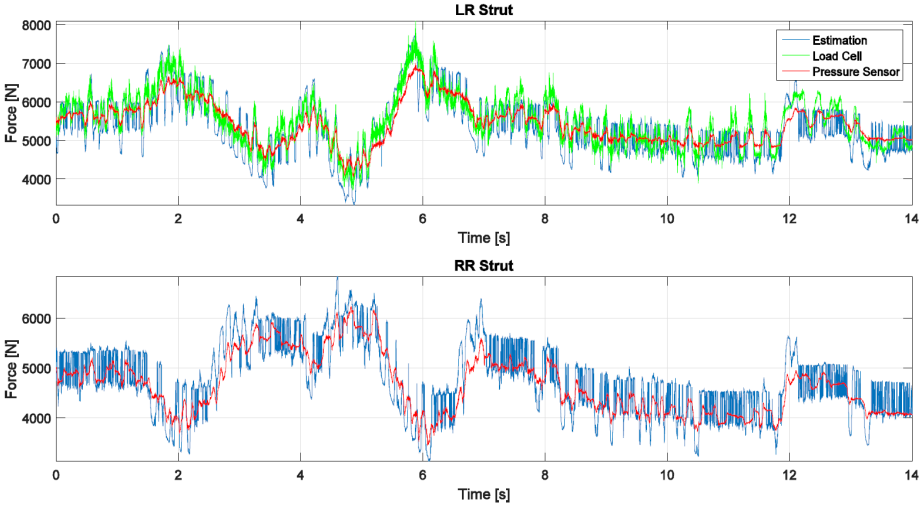

None the less, the estimated values provide very good information for improving control systems such as ABS, ESC, etc. where the vertical suspension or tyre forces can be used to improve control. The DLC test also excites the roll degree of freedom with almost no time for steady state response. Therefore, the roll acceleration during this test is high. Therefore, the effect of neglecting the roll inertia in the formulations seems to have very small effect on this accuracy of the estimators.

Figure 8 Experimental results of the estimated inertial parameters during a DLC at different speeds (see online version for colours)

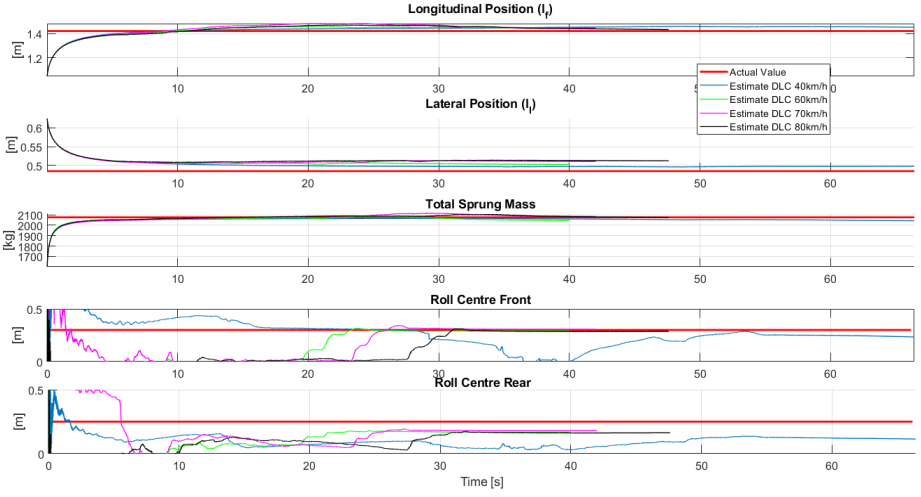

The DLC was also conducted at entry speeds of 40, 60, 70 and 80 km/h, which corresponds to maximum lateral accelerations of 0.23 g, 0.42 g, 0.52 g and 0.6 g respectively. Figure 8 shows the results of the parameter estimation for all of the DLC tests conducted. The results show that the estimated parameters converge to close to the actual values. The estimation errors are tabulated in Table 2. The longitudinal position is within 2.5% of the actual value, while the lateral position is within 6% and the total mass within 2%. The lateral position is more susceptible to smaller errors in the mass estimation due to the much smaller distance between left and right struts compared to the front and rear struts.

Table 2 Percentage error of estimated for different entry speeds of a DLC manoeuvre

Speed	*CoM long pos* (l_f)	*CoM lat pos* (l_l)	*Total sprung mass*	*Roll centre height front* (h_{rf})	*roll centre height rear* (h_{rr})
40 km/h	2.2%	2.7%	1.6%	22.2%	54%
60 km/h	1.6%	3.7%	1.5%	2.8%	32%
70 km/h	1.7%	5.2%	0.39%	2.3%	28%
80 km/h	0.8%	5.6%	0%	4.7%	33.2%

The results in Figure 8 includes the full test which consists of a large portion of straight driving before the actual manoeuvre takes place. The roll centre estimate changes slowly in the beginning until the manoeuvre starts (for example at 20 s for 60 km/h) thereafter the estimate converges to the actual value. The actual value of the roll centre is very difficult to determine due to its definition and the fact that it changes as the body rolls. An approximation can be made using the geometry of the suspension components (Gillespie, 1992; Jazar, 2017), results in values of 0.3 m and 0.25 m for the front and rear

roll centre respectively. This uncertainty results in slightly larger estimation errors which decrease as the lateral acceleration increases. The increase in accuracy is expected as there are larger excitations to use in the estimation algorithm. The rear roll centre is within 5% of the value approximated from the suspension geometry at lateral accelerations higher than 0.4 g. The rear roll centre error is however much larger. While the error does decrease as acceleration increases, the estimate, heights are in the range of 0.17–0.18 m rather than 0.25 m. It is difficult to say which value is closer to the true actual value. However, the UKF estimated value can easily be used in a vehicle model which uses the same formulation of the estimator to make predictions or be used for control purposes.

Figure 9 Experimental results of the estimated inertial parameters using better initial estimate (see online version for colours)

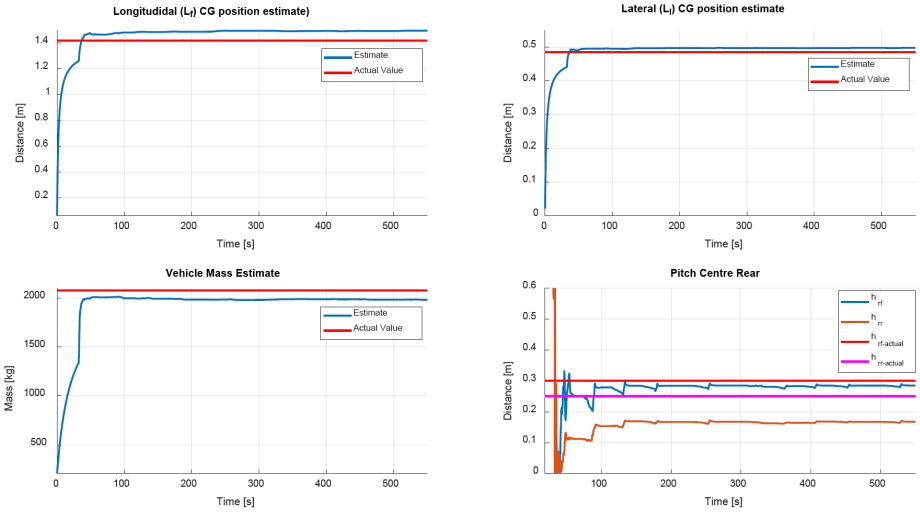

Table 3 Mean, standard deviation and maximum deviation of estimated for the front and rear roll centre heights while performing multiple DLC manoeuvres

	Roll centre height front (h_{rf}) *[m]*	*Roll centre height rear* (h_{rr}) *[m]*
Mean	0.283	0.17
Standard deviation	0.002	0.002
Maximum deviation	0.010	0.006

The convergence of the estimator takes several seconds until an acceptable estimate of the values are obtained. This however can be improved by initialising the estimator with better estimates. The stability of the estimator is tested by running the estimator through multiple runs of all the DLC tests conducted at 40, 60, 70, 80 km/h in one estimation. This was done by simply appending the data for each run in a single data structure The estimator was run through the appended data twice to increase the number of runs. The results are shown in Figure 9. The results show that the estimate converges to the same estimates as previously obtained for signel DLC manoeuvres. The standard deviation and maximum deviation is shown in Table 3, determined after 200 s when convergence

occurs. The estimates remain stable throughout convergence and never show any large deviations from the actual converged values.

4.3 Rural and city driving

Data was recorded as the vehicle was driving on a typical rural, city and highway roads for a period of 1,750 s. The test was conducted using typical driving behaviour of a conservative driver. In the rural driving speeds of 100 km/h were reached with very little longitudinal acceleration and considerable vertical excitation due to uneven road. During city driving low speeds below 60 km/h were reached with stop start conditions. During highway driving constant speeds were reached of 120 km/h with very little excitation at all. Figure 10 shows the measured longitudinal and lateral acceleration from the rural driving. From the figure it can be observed that the measured signals are very noisy. This is mainly due to the vehicle itself, with the accelerometers measuring engine, gearbox as well as other body vibrations. The measurements were used as is in the previous tests without adding filtering. A filtered plot is provided to determine the maximum acceleration experienced by the vehicle. The maximum longitudinal acceleration is less than 0.2 g (2 m/s^2) and lateral acceleration less than 0.35 g (3.5 m/s^2). These accelerations were the highest reached of all driving scenarios. As the test was not performed at a testing facility but on a public road, the outriggers on the vehicle were removed. Therefore, the mass of the vehicle for this test is lower than the other tests. The estimator was run through the reiving scenarios twice totalling 3,500 s of data to determine stability of the estimator.

Figure 10 Measured longitudinal and lateral acceleration during a 340 s rural driving test (see online version for colours)

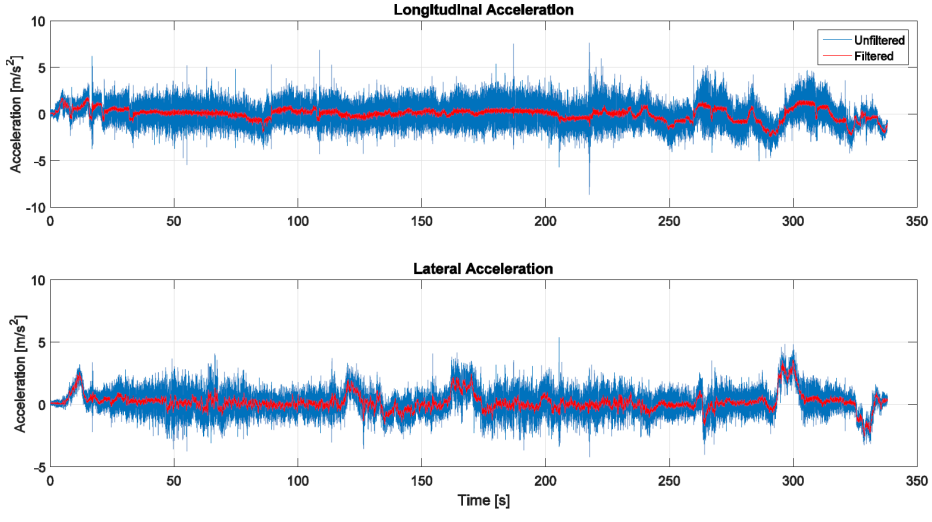

The data in Figure 11 shows the error in the longitudinal and lateral centre of mass location is less than 3.5% and 2.5% respectively. The sprung mass is estimated within 5%. The estimates of the roll and pitch centres are shown in Table 4. The table shows that the estimates are very stable with less than a 5 mm standard deviation after the estimates converge. The error on the front and rear roll centre is 26% and 28%. The error in the roll

centre is rather large however since the test has very little excitation this is to be expected. It should be noted however that the rear roll centre height is the same as found in the DLC manoeuvres. The exact cause of the deviation for the front roll centre height from the DLC manoeuvres is not exactly known. In both scenarios the estimates are very stable which could lead to the conclusion that the deviations are due to changes in the setup or suspension, such as gas volumes or suspension friction since the tests were conducted at different dates.

Figure 11 Actual vs. estimated parameters during a rural driving test (see online version for colours)

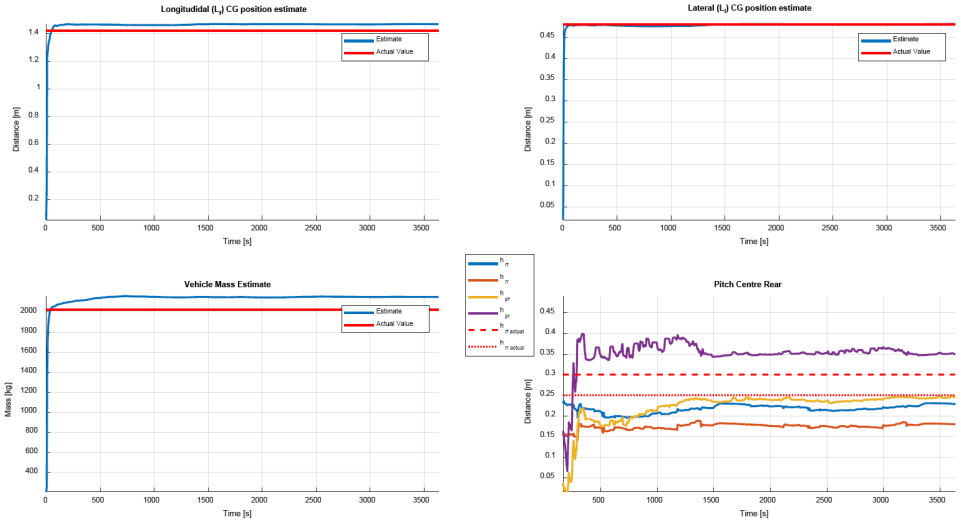

Table 4 Mean, standard deviation and maximum deviation of estimated for the roll and pitch centre heights during normal driving conditions

	Roll centre height front (h_{rf}) [m]	*Roll centre height rear (h_{rr}) [m]*	*Pitch centre height left (h_{pl}) [m]*	*Pitch centre height right (h_{pr}) [m]*
Mean	0.22	0.177	0.24	0.35
Standard deviation	0.0058	0.0034	0.0041	0.0049
Maximum deviation	0.010	0.008	0.0097	0.013

4.4 Real time

The estimators are to be used in real time estimation of the suspension forces and vehicle mass properties. The algorithms were run on an i5-3470 at 3.2 GHz. The code was run on un-optimised MATLAB code running the Kalman filters at 100 Hz. The code was found to run at 5 times faster than real-time. It is expected that optimised code running on C/C++ code will be able to run in real-time on a slower embedded system.

5 Conclusions

In this paper two estimators have been developed. The first is a linear Kalman filter to estimate the suspension displacements and velocities which can be used as inputs to a suspension model to determine the suspension forces. The estimator uses simple and cheap measurements to generate these estimates. The estimator is shown to give low noise estimates of the displacement and velocities of the suspension and that these can be used to estimate the suspension forces accurately. The estimated suspension forces are used as inputs to a second nonlinear unscented Kalman filter to estimate the location and mass of the sprung centre of mass of the vehicle. The estimator also estimates the front and rear roll centres as well as a left and right pitch centres in real time. The estimators have been validated using experimental data on a Land Rover Defender performing various manoeuvres and driving over different terrains. The estimator shows that it can estimate the centre of mass position and mass of the sprung mass accurately within 5% of the actual value for various driving conditions. The accuracy of the roll centre positions is significantly larger, especially for the rear roll centre. The larger errors could be due to the actual values used which is approximated from the suspension geometry and therefore not the actual locations. However, the estimates of the suspension forces, rather than using the lateral acceleration and load transfer model, can be used directly in control systems which can benefit from the knowing the vertical force on the tyres or suspension forces. Whether the suspension forces or the vehicle parameters, in conjunction with a vehicle model, is used for control purposes, the real time estimation of these values can be used to improve the control of systems such as ABS, ESC, suspension-control, torque vectoring, etc., therefore, improving the handling and safety of the vehicle.

References

Chu, W., Cao, K., Li, S., Luo, Y. and Li, K. (2013) 'Vehicle mass estimation based on high-frequency-information extraction', *IFAC Proceedings Volumes*, Vol. 46, No. 21, pp.72–76.

Di Cairano, S., Tseng, H.E., Bernardini, D. and Bemporad, A. (2013) 'Vehicle yaw stability control by coordinated active front steering and differential braking in the tire sideslip angles domain', *IEEE Transactions on Control Systems Technology*, Vol. 21, No. 4, pp.1236–1248.

Gillespie, T.D. (1992) *Fundamentals of Vehicle Dynamics*, Vol. 114, SAE International, USA.

Hahn, J.O., Rajamani, R. and Alexander, L. (2002) 'GPS-based real-time identification of tire-road friction coefficient', *IEEE Transactions on Control Systems Technology*, Vol. 10, No. 3, pp.331–343.

Holm, E.J. (2011) *Vehicle Mass and Road Grade Estimation Using Kalman Filter*, Linköping University, Sweden.

Huang, X. and Wang, J. (2012) 'Adaptive vehicle planar motion control with fast parameter estimation', *2012 IEEE 51st Annual Conference on Decision and Control (CDC)*, December, pp.5034–5039, IEEE.

Huang, X. and Wang, J. (2013) 'Center of gravity height real-time estimation for lightweight vehicles using tire instant effective radius', *Control Engineering Practice*, Vol. 21, No. 4, pp.370–380.

International Organisation for Standardisation (1999) *ISO 3888-1: Passenger Cars – Test Track for a Severe Lane-Change Manoeuvre – Part 1: Double Lane-Change*, The International Organisation for Standardisation.

Jazar, R.N. (2017) *Vehicle Dynamics: Theory and Application*, Springer.

Julier, S.J. and Uhlmann, J.K. (1995) 'A new approach for filtering nonlinear systems', *Proceedings of the American Control Conference*, pp.1628–1632.

Julier, S.J. and Uhlmann, J.K. (1997) 'A new extension of the Kalman filter to nonlinear systems', *Proc. of AeroSense: The 11th Int. Symp. on Aerospace/Defence Sensing, Simulation and Controls*.

Kalman, R.E. (1960) 'A new approach to linear filtering and prediction problems', *Transactions of the ASME: Journal of Basic Engineering*, Vol. 82, No. 1, pp.35–45.

Kim, I., Kim, H., Bang, J. and Huh, K. (2013) 'Development of estimation algorithms for vehicle's mass and road grade', *International Journal of Automotive Technology*, Vol. 14, No. 6, pp.889–895.

Madhusudhanan, A.K., Corno, M., Arat, M.A. and Holweg, E. (2016) 'Load sensing bearing based road-tyre friction estimation considering combined tyre slip', *Mechatronics*, Vol. 39, pp.136–146.

Rozyn, M. and Zhang, N. (2010) 'A method for estimation of vehicle inertial parameters', *Vehicle System Dynamics*, Vol. 48, No. 5, pp.547–565.

Rubin, D. and Arogeti, S.A. (2015) 'Vehicle yaw stability control using active limited-slip differential via model predictive control methods', *Vehicle System Dynamics*, Vol. 53, No. 9, pp.1315–1330.

Sandu, C., Kolansky, J., Botha, T.R. and Els, P.S. (2015) 'Multibody dynamics techniques for real-time parameter estimation', *Advanced Autonomous Vehicle Design for Severe Environments*, Vol. 44, pp.221–241.

Solmaz, S., Akar, M., Shorten, R. and Kalkkuhl, J. (2008) 'Real-time multiple-model estimation of centre of gravity position in automotive vehicles', *Vehicle System Dynamics*, Vol. 46, No. 9, pp.763–788.

Tchamna, R. and Youn, I. (2013) 'Yaw rate and side-slip control considering vehicle longitudinal dynamics', *International Journal of Automotive Technology*, Vol. 14, No. 1, pp.53–60.

Yoon, J., Kim, D. and Yi, K. (2007) 'Design of a rollover index-based vehicle stability control scheme', *Vehicle System Dynamics*, Vol. 45, No. 5, pp.459–475.

Nomenclature

Variable	*Definition*	*Units*
Z_{aij}	Vertical height at corner *ij*	[m]
aij	Unsprung mass ($a = u$) or sprung mass ($a = s$) at corner of vehicle $i = l$ (left), r (right) and $j = f$ (front), r (rear)	
$\dot{Z}_{aij}$	Vertical velocity at corner *ij*	[m/s]
$\ddot{Z}_{aij}$	Vertical acceleration of corner *ij*	[m/s^2]
t	Time	[s]
δ_{ij}	Suspension deflection at corner *ij*	[m]
$\dot{\theta}_r$	Roll velocity of vehicle body	[rad/s]
$\dot{\theta}_p$	Pitch velocity of vehicle body	[rad/s]
$\dot{\delta}_{ij}$	Suspension velocity at corner *ij*	[m/s]
F_{zij}	Vertical force of suspension at corner *ij*	[N]
F_{bounce}	Total force on sprung body from suspension	[N]
m	Mass of vehicle	[kg]
$A_{x\mathrm{CoM}}$	Vehicle longitudinal acceleration of centre of mass	[m/s^2]
$A_{y\mathrm{CoM}}$	Vehicle lateral acceleration of centre of mass	[m/s^2]
l_w	Track width of vehicle	[m]
l_f	Distance from front axle to centre of mass	[m]
l_r	Distance from rear axle to centre of mass	[m]
l	Distance between front and rear axle	[m]
l_l	Distance from left tyres to centre of mass	[m]
m_{ij}	Point mass at corner *ij*	[kg]
h_{pi}	Distance of pitch centre to centre of mass $i = l$ (left), r (right)	[m]
h_r	Distance of roll centre to centre of mass	[m]
h_{rj}	Distance of roll centre to centre of mass at axle $j = f$ (front), r (rear)	[m]
$\boldsymbol{X}_k$	State vector at time k	
$\boldsymbol{F}$	State transition model	
$\boldsymbol{U}_k$	Input matrix	
$\boldsymbol{Y}_k$	Measurement matrix	
$\boldsymbol{H}$	State observation model	
$\boldsymbol{B}$	Input model	
$\boldsymbol{P}_k$	Covariance matrix at time step k	
$\boldsymbol{\chi}^*_{k\|k-1}$	Propagated sigma points	
W_i^m	Measurement weight	
W_i^c	Process noise covariance weights	
$\boldsymbol{R}_n$	Measurement covariance noise matrix	
$\boldsymbol{R}_v$	Process covariance noise matrix	
$\boldsymbol{\gamma}_k$	Measurement vector for UKF	